Finite Element Modeling of Capacitive Micromachined Ultrasonic Transducers

Goksen G. Yaralioglu*, Baris Bayram, Amin Nikoozadeh, B.T. Pierre Khuri-Yakub
E.L. Ginzton Laboratory, Stanford University, Stanford, CA 94305

ABSTRACT

Transducers based on piezoelectric crystals dominate the biomedical ultrasonic imaging field. However, fabrication difficulties for piezoelectric transducers limit their usage for complex imaging modalities such as 2D imaging, high frequency imaging, and forward looking intravascular imaging. Capacitive micromachined ultrasonic transducers (CMUTs) have been proposed to overcome these limitations and they offer competitive advantages in terms of bandwidth and dynamic range. Further, the ease of fabrication enables manufacturing of complex array geometries. A CMUT transducer is composed of many electrostatically actuated membranes. Earlier analysis of these devices concentrated on an equivalent circuit approach, which assumed the motion of the membrane was approximated by a parallel plate capacitor. Finite element analysis is required for more accurate results. In this paper, we present the finite element model developed to evaluate the performance of the CMUTs. The model is composed of a membrane radiating into immersion medium. Electrostatic actuation is added on using electromechanical elements. Symmetry boundary conditions are imposed around the sidewalls of the finite element mesh, so that the model reflects the properties of a cell driven with the same phase as its neighboring membranes in an infinitely large array. Absorbing boundaries are implemented one wavelength away from the membrane to avoid reflections from the end of the finite element mesh. Using the model, we optimized the membrane radius, membrane thickness and gap height. Our optimized designed yielded a center frequency of 13 MHz with hundred percent bandwidth. A maximum output pressure of 20 kPascal per volt was obtained.

Keywords: Capacitive micromachined ultrasonic transducer (CMUT), finite element analysis (FEA)

1. INTRODUCTION

Capacitive micromachined ultrasonic transducers are one of the few MEMS technologies that promise near future commercial success[1]. Capacitive sensors have long been used for the transmission and reception of sound waves. However, only recently, capacitive transducers that are fabricated using micromachning techniques become a competitor for piezoelectric devices. MEMS technologies are the main enabling tools for this advancement. Using silicon micromachining techniques it is possible to fabricate very small gap heights and therefore to obtain very high electric fields which is essential for transmitting high pressures and detecting very small displacements. Moreover, using only photolithography, one can build very complex array geometries which are otherwise not possible using piezoelectric transducers.

A CMUT transducer is composed of many membranes. The membranes, which are suspended over a small gap, are usually made of either silicon or silicon nitride. A metal electrode on the membrane and the doped substrate form the top and the bottom electrodes, respectively. If an AC voltage in addition to a DC bias is applied between the electrodes, the membrane starts vibrating and generating sound waves into the medium. For reception, the membrane is again biased by a DC voltage and if sound waves impinge on the device, the capacitance between the top and bottom electrodes generate current at the frequency of the incoming sound waves.

The growing interest in the CMUT technology for biomedical imaging applications increased the modeling efforts for these devices. Initially equivalent circuit modeling based on parallel plate approximation has been used[2]. In this approach the membrane is assumed to be moving parallel to the substrate and the equivalent circuit parameters are

* Corresponding author: goksenin@stanford.edu

Medical Imaging 2005: Ultrasonic Imaging and Signal Processing,
edited by William F. Walker, Stanislav Y. Emelianov, Proc. of SPIE Vol. 5750
(SPIE, Bellingham, WA, 2005) · 1605-7422/05/$15 · doi: 10.1117/12.595619

calculated using this assumption. This approach has been improved by various authors[3,4] to get a better estimate of the transducer parameters such as bandwidth, output pressure and sensitivity.

However, calculations involving complex membrane structures, cross-talk and evaluation of radiation pattern necessitate the use of finite element analysis. FEA has been employed for successfully for the characterization of different aspects of CMUTs. For example, FEA tools have been used for the calculation of quasi-static membrane deflection under bias voltage[5-8]. In addition to quasi-static models, harmonic analysis has also been used. These models have been used to predict the output pressure[3] as well as the cross-talk[9] between the membranes. There are also FEA models developed to investigate the cross-talk[10] and non-linear behavior of CMUTs[11,12] through time domain analysis.

In this paper, we present our 2D FEA modeling efforts for CMUTs. The scope of this paper is limited to the harmonic analysis.

2. FEM MODELING

In all our calculations, we have used commercially available finite element software (ANSYS8.0). The membrane was modeled by plane (PLANE42) elements. The electrical ports were added to the model using transducer (TRANS126) elements. For immersion medium, fluid (FLUID29) elements were used. The fluid mesh was terminated by using absorbing boundary element (FLUID129) or using boundary admittance method.

2.1. Modeling of Membrane

The first CMUTs were fabricated using sacrificial etching technique where the membrane is made of silicon nitride thin film[2]. Silicon nitride forms an isotropic film, however it is difficult to control and measure its material parameters. To overcome these difficulties, wafer-bonding technique was developed. In this technique an SOI wafer is bonded over oxide cavities and handle part of the SOI wafer is removed. This provides membranes made of single crystal silicon. Silicon is anisotropic and its elastic material parameters are well known. For silicon membranes, device properties such as collapse voltage and resonance frequency are dictated by the average of anisotropic material properties. In ANSYS, it is possible to include anisotropy for 3D analysis. However for 2D models, average material properties should be used. In this section, we will investigate the effect of silicon anisotropy on membrane properties and find equivalent isotropic material properties for 2D analysis.

Various membrane geometries, such as circular, rectangular, hexagonal, have been used in CMUT transducers. Fig 1 shows FEM models for different membrane geometries.

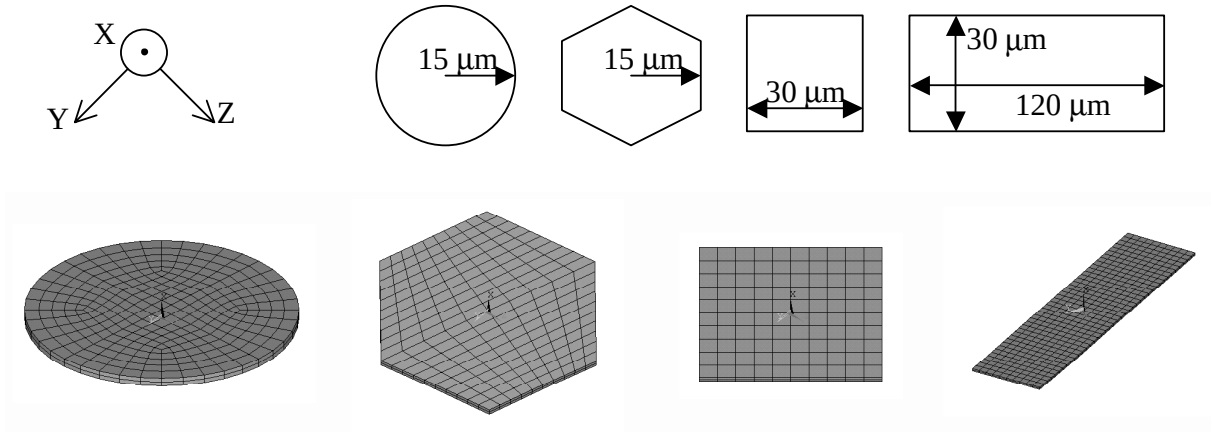

Figure 1. Various CMUT membrane geometries. Top figures show the dimensions of the membranes, bottom figures show the FEM mesh. The mesh density is reduced for visibility. The membranes are made of (100) SOI wafer. Top figures show the membrane orientation when $\theta=0$ (θ is the rotation about X axis). The membrane thickness is 1 μm.

The results of the resonance frequency calculations of the membranes are shown in Fig.2. As expected the curves are periodic with the period of 90 degrees due to two fold symmetry of the cubic silicon material. The resonance frequencies are normalized. The resonance frequency of the square and rectangular membranes vary 1 and 8 percent, respectively, whereas the variation on the hexagonal membrane resonance frequency is less than 0.1 percent.

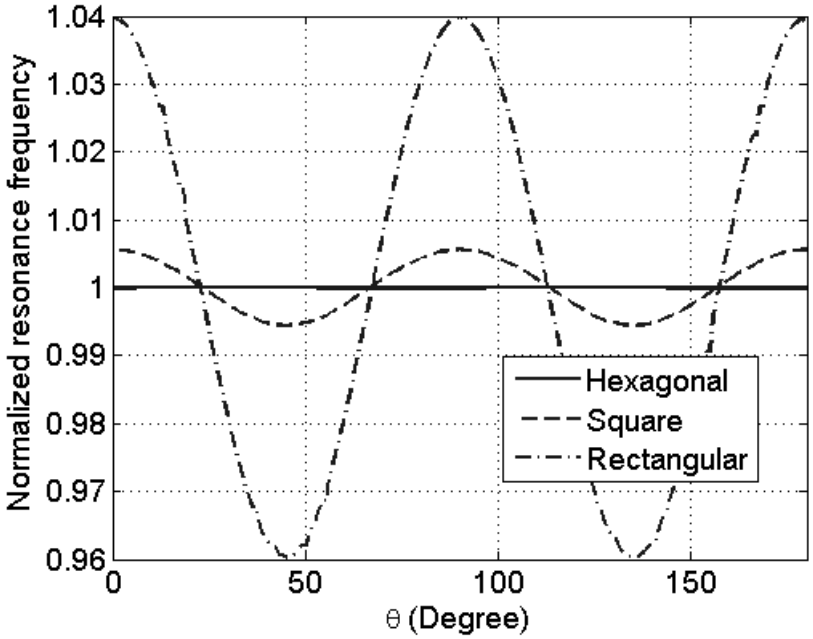

Figure 2. Resonance frequencies of the membranes shown in Fig 1. The resonance frequencies are normalized by 15.91 MHz, 14.94 MHz and 9.49 MHz for hexagonal, square and rectangular membranes, respectively. Silicon material properties: c_{11}=165.7 Gpa, c_{12}=63.9 Gpa, c_{44}= 79.56 Gpa, density=2332 kg/m^3.

The resonance frequency of the circular membrane, which was calculated to be 16.93 MHZ, is independent of the orientation angle, θ. We used the circular membrane to find the equivalent isotropic material properties for (100) silicon surface. The material properties of a 2D axisymetric model was adjusted to get the as same properties as the 3D circular membrane discussed above. The resonance frequency and the deflection under a DC load of the planar model matched to those of 3D model by using appropriate Young's modulus and Poisson's ratio. Our calculations revealed that isotropic Poisson ratio is 0.173 and Young's modulus is 148.2 Gpa. These values match very well with the values reported in reference 14.

2.2. Modeling of electrical ports

The electrical ports were included in the model by using transducer elements (TRANS126) of ANSYS. These elements are parallel plate capacitors. They can be attached between two nodes and under an applied electrical field, electrostatic forces proportional to the field are applied to these nodes. We divided the electrostatic gap into smaller segments and the electrostatic attractive forces in each segment are modeled by a transducer element. A schematic drawing of the FEM mesh is shown in Fig. 3.

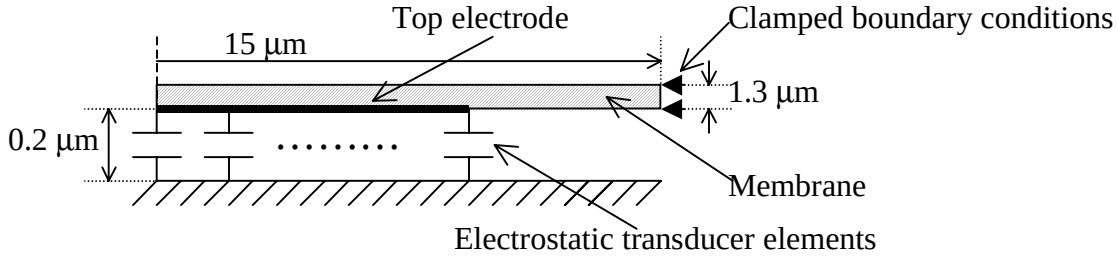

Figure 3. FEM model used for the electrostatic gap. The membrane is made of silicon. The radius of the top electrode is half of the membrane radius. The top electrode is assumed to be on the bottom surface of the membrane.

Combined with the transducer elements, one can easily find the collapse voltage of the membrane. In addition, the same model can be used to calculate the input impedance of the device in vacuum by performing harmonic analysis. The collapse voltage of the membrane shown in Fig. 3 is 135.4 V. Fig. 4 shows the imaginary part of the input impedance when the membrane is biased at 90 percent of its collapse voltage.

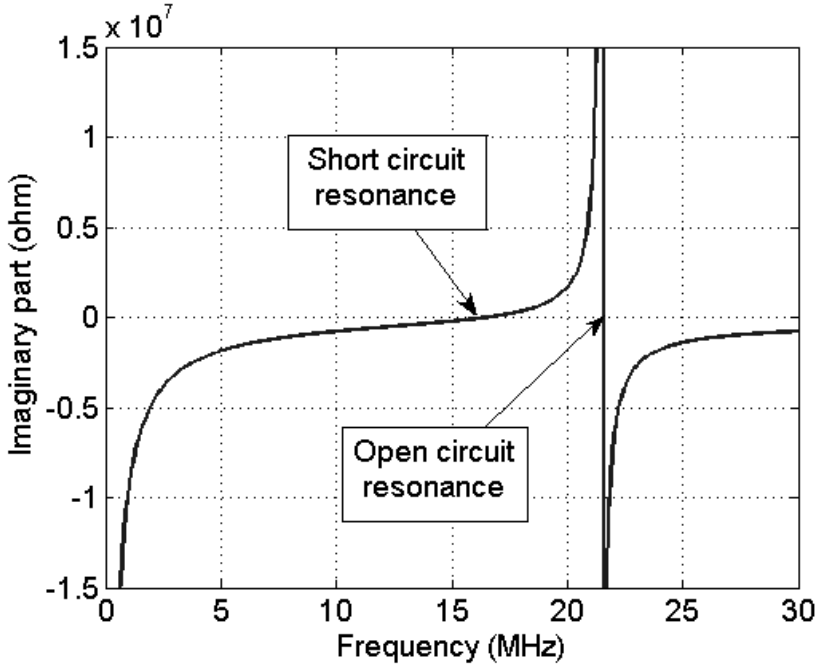

Figure 4. Imaginary part of the electrical impedance of the transducer shown in Fig. 3. Since there is no loss in the device the real part is zero.

The important features of the electrical input impedance are open and short circuit resonance frequencies. The maximum vibration amplitude is achieved at the short circuit resonance frequency where the amplitude of the impedance is zero. Without electrical field, the native resonance frequency of the membrane is at a higher frequency which is 21.71 MHz for the membrane shown in Fig. 3. The downshift of the frequency where the maximum displacement is achieved is called spring softening. On the other hand, at the open circuit resonance frequency, the amplitude of the impedance goes to infinity. This is the frequency where the membrane resonates without electrical field.

2.3. Modeling of immersion devices

Previously we have shown 3D models of membranes operating in fluid medium[3]. We have modeled one row of an array element with symmetry boundary conditions at the top and bottom surfaces. One can further simplify this approach by applying symmetry boundary conditions around a square unit cell. This model will assume an infinitely large transducer, which is composed of replication of unit cell in lateral dimensions. The latter model is basically a

membrane that is radiating into a rectangular wave-guide. This approach has been also used by other authors[4]. The rectangular wave-guide can be further replaced by a cylindrical wave-guide without changing the radiation conditions much. This results in a small 2D FEM model and fast simulation time. Fig. 5a shows a 2D model where a circular membrane is radiating into a cylindrical wave-guide. The fluid column was meshed using FLUID29 elements of ANSYS. The radius of the fluid column was chosen to reflect the total area of the unit cell including the nonmembrane regions such as posts of the membrane. The fluid-solid interaction was turned on over the surface of the membrane. The electrostatic gap was modeled by using transducer elements (TRANS126). We also applied absorbing boundaries at the top of the fluid region to simulate radiation into half space. For the implementation of absorbing boundaries there are two alternative methods in ANSYS. One can either use the built-in absorbing boundary elements (FLUID30) or assign appropriate impedance to the boundary to absorb the incoming waves. The implementation is relatively involved for the first method since the absorbing boundary should lie on a circle. Therefore, we used the second method in the calculations. Fig. 5b shows the average pressure over the membrane plane including the non-membrane region. We used the same membrane that was described in section 2.1. The maximum output pressure is 20 kPa/V. The 3dB bandwidth of the transducer is slightly over 100 percent, from 7.93 MHz to 22.42 MHz.

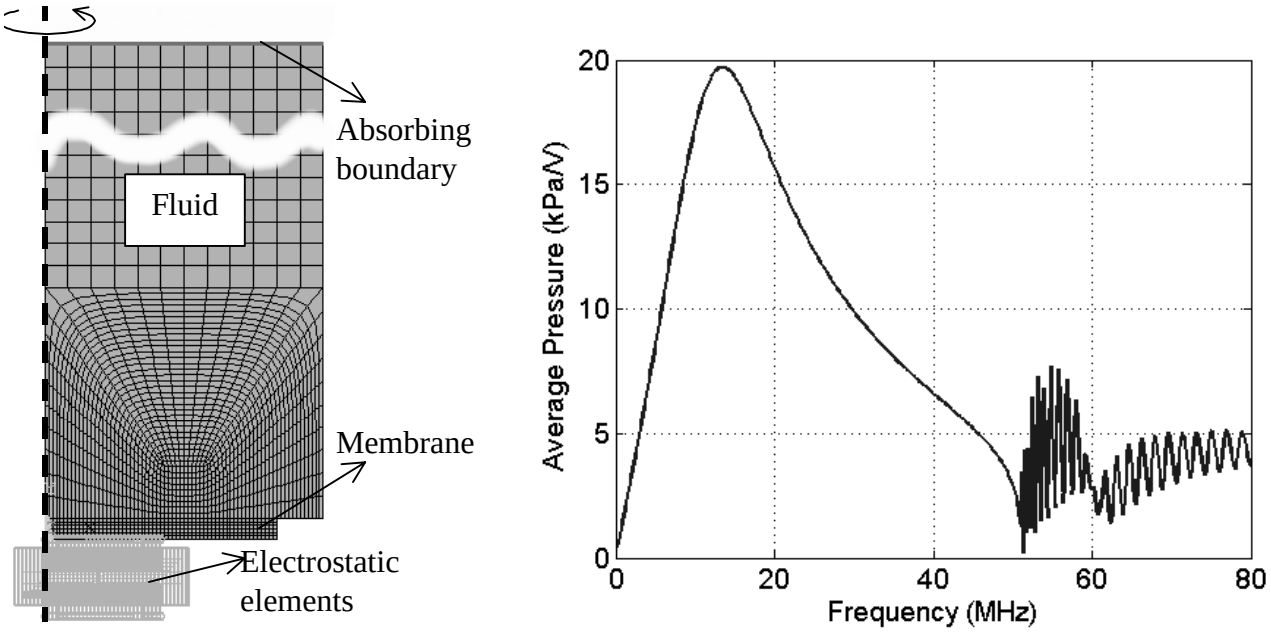

Figure 5. (a) FEM mesh. The height and the radius of the fluid column is 600 μm and 18 μm, respectively. The membrane radius is 15 μm. The gap height is 0.2 μm. (b) Output pressure. The membrane is biased at 108.3 V.

One point to note is that frequencies above 50 MHz, there are standing wave pattern occurs in the wave guide. Below this frequency, the wave fronts are parallel to the absorbing boundary and the absorbing boundary works very well. However, above certain frequency waves start propagating oblique to the absorbing boundary and they cannot be fully absorbed. Fig. 6 shows the field profile in the fluid. The main reason for this is that for that particular geometry, the cut-off for the higher order modes of the wave guide is around 50 MHz. Above this frequency, the wave guide can support waves going at an angle. This frequency can be determined by the following equation:

$$f_c = 1.22 \frac{v_L}{2r_{out}}$$

where v_L is the sound velocity in water. Since the absorbing boundary does not work very well above this frequency, an higher order absorbing boundary is needed or one can use a long lossy fluid part to eliminate the reflections from the end of the mesh. Never the less, around the operation frequency of the membrane the results are accurate.

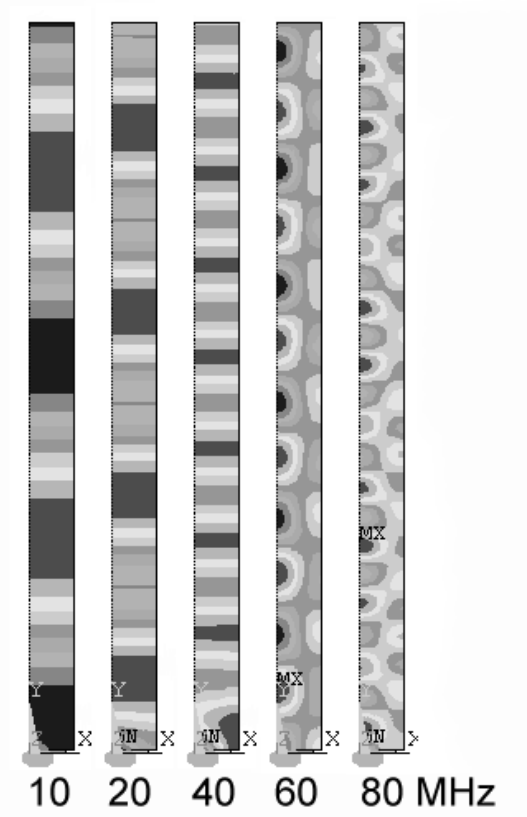

Figure 6. (a) Real part of pressure field in the fluid column. The height and the radius of the column is 600 μm and 18 μm, respectively. The membrane is located at the bottom part of the fluid column.

3. FEM RESULTS

Using the FEM model described above one can investigate various aspects of the CMUT transducers. First, we checked the effect of gap height on the device performance. Fig. 7 shows the output pressure per volt as a function of gap distance. The electrical field inside the cavity is dictated by the gap height and the DC bias. The CMUTs are usually biased close to their collapse voltages. Reducing the gap height reduces the collapse voltage. However, the electrical field increases if the membrane is biased at the same percentage of the collapse voltage as the gap height decreases. This results in increased output pressure per volt. On the other hand, the total maximum pressure, of course, is limited by the total gap height. However, usually the electrical pulse that can be applied to the device is limited. Therefore very large gap heights are not practical. To get higher output pressure one needs to increase the bias voltage and therefore the collapse voltage. But increasing collapse voltage by increasing the gap height will not increase the output pressure. Therefore, the collapse voltage should be increased by optimizing the other membrane parameters such as the stiffness.

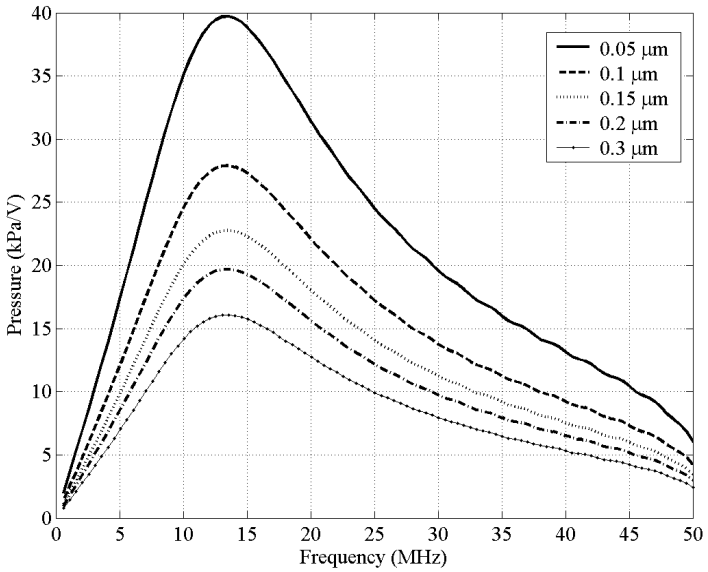

Figure 7. Dependence of output pressure to the gap distance.

We also used the same model to investigate the effect of various membrane parameters. Fig. 8 shows the output pressure as a function of various membrane dimensions. The membranes used in the simulations have the same resonance frequencies in air (21.71 MHz). In the calculations, the ratio of the membrane area to the total area is also kept constant (0.7) by adjusting the outer radius of the model.

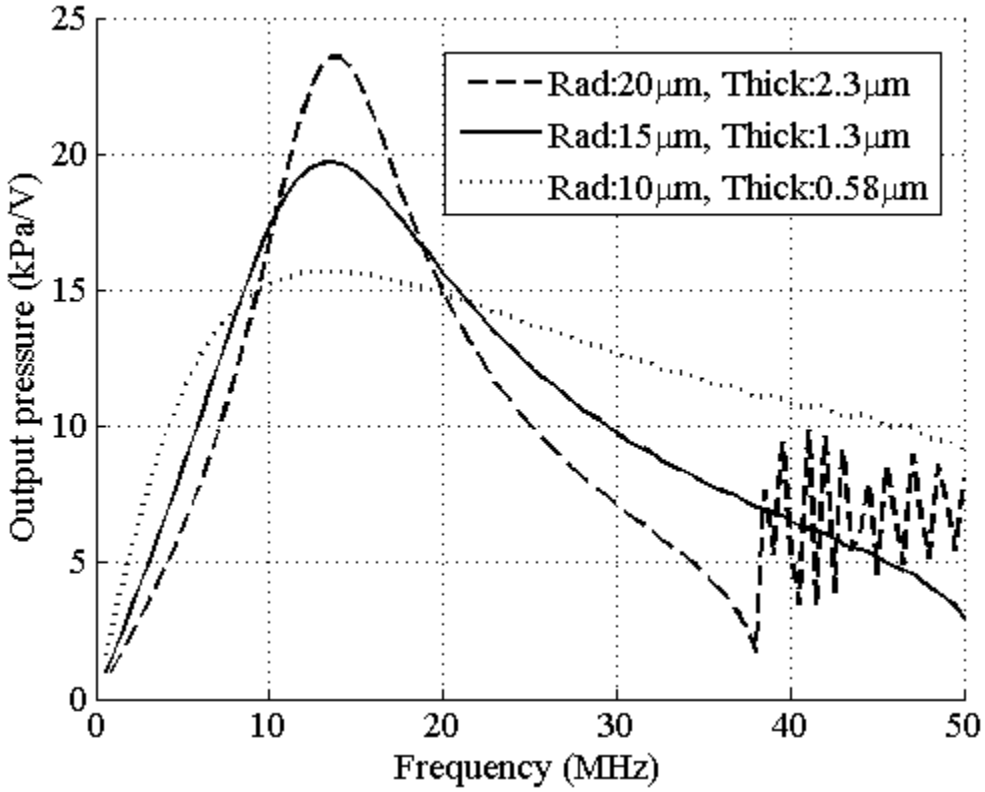

Figure 8. Output pressure for various membrane dimensions. The ratio of the membrane area to the total area is 70 percent. The collapse voltages of the membranes are 91.5, 135.4, and 177.6V. The bias voltage was set equal to the 80 percent of the collapse voltage for each membrane.

As the membrane stiffness increases the bandwidth decreases as shown in Fig 8. The softer membrane generated the maximum bandwidth, since the mechanical membrane impedance is small compared to the radiation impedance over a broader frequency band. But, the output pressure is low compared to the other membrane sizes because of the low bias voltage that is determined by the collapse voltage. The stiffer membrane generated higher output pressure with a narrower bandwidth. Another, important observation was that the fluid loading reduced the resonance frequency at the same rate for all of the membrane sizes. But the output pressure per volt increases for stiffer membranes due to the increased collapse voltage. Note that, the membranes are biased at 80 percent of their collapse voltages. For 20 μm membrane, the standing waves start appearing at 38 MHz which can be estimated using equation (1) for r_{out}=24.08 μm.

FEM analysis is especially useful when the geometries are complex. The above modeling approach can be also used for membranes with complex geometries. Fig. 9 shows a membrane with a thicker central portion. The central part allows more piston like motion. This increases the average membrane displacement and consequently the output pressure. Membranes with central masses were demonstrated previously at low frequencies (around 1MHz) to get higher bandwidth and output pressures[15]. This design also allows another parameter to adjust the stiffness of the membrane. It is possible to fabricate membranes with the same radius and thickness but with different stiffnesses.

The radius of the central portion of the membrane shown in Fig 9 is 8 μm and the thickness of this part is 3.2 μm. The resonance frequency in air is same as that of the membrane shown in Fig. 5. The gap distance is 0.134 μm, which was adjusted to get the same collapse voltage, 135.4 as before. The output pressure per volt is depicted Fig. 10. As expected, the amplitude of the pressure increased to 37.6 kPa/V but the bandwidth is dropped to 59%. Also note that the resonance frequency increased to 16.15 MHz. Previously, it was 13.5 MHz. This is due to the fact that the fluid mass loading is less effective on the membrane with the central mass, since the mass of this membrane is relatively larger. We also simulated the structure where the mass is on top of the membrane and gotten very similar pressure curve shown in Fig. 9.

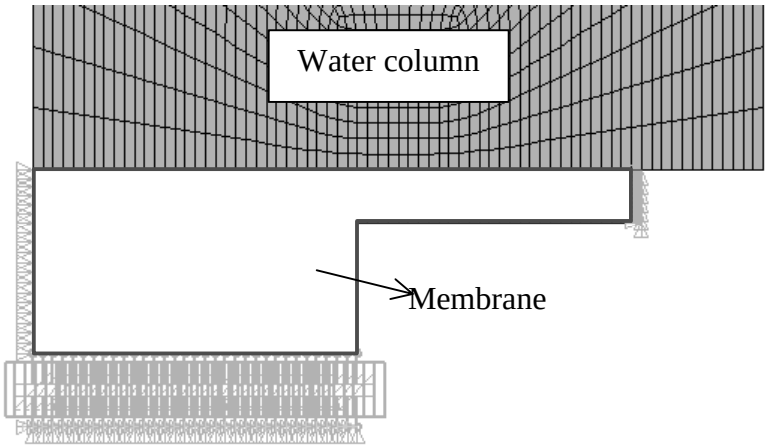

Figure 9. Membrane with a central mass. The thickness of the central mass of the membrane is 3.2 μm, the membrane is 1.3 μm thick. The radius of the central mass is 8 μm. This membrane has the same resonance frequency (21.71MHz) in air as the membrane depicted in Fig. 5. The gap distance is 0.134 μm.

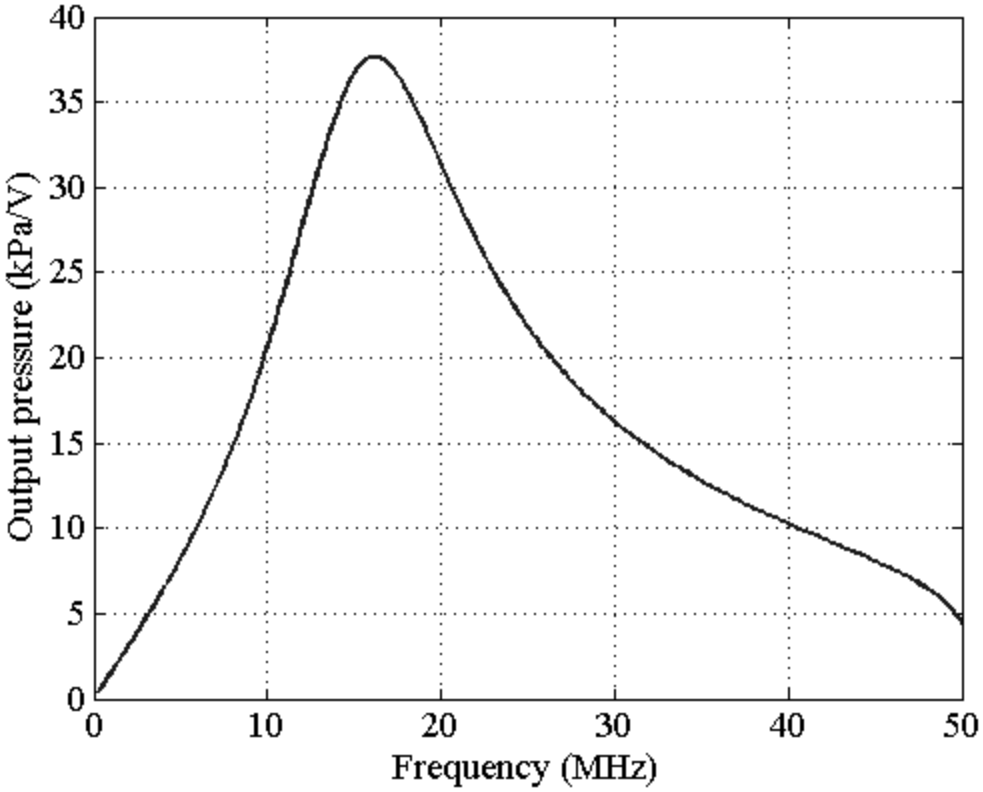

Figure 10. Output pressure of the membrane shown in Fig. 9.

CONCLUSION

We have demonstrated FEM calculations for CMUTs. The electrostatic gap is included in the model using transducer elements. The gap height can be optimized to maximize the output pressure. Decreasing the gap increases the output pressure per volt. However, the maximum pressure that can be obtained from a CMUT membrane is limited by the gap height if there is no limitation on the applied pulse amplitude. If the pulse amplitude is limited, then one can try to increase the collapse voltage to be able to apply more DC bias on the transducer. The collapse voltage should not be increased by increasing the gap height since this will reduce the total pressure output as demonstrated. Using a stiffer membrane might increase the collapse voltage. But this will reduce the bandwidth. Therefore, the design of a CMUT must be done carefully, by considering both pressure output and bandwidth. Output pressure and bandwidth impose contradicting restrictions on the device parameters. Using a membrane with a central mass enables adjusting membrane stiffness and mass separately. This approach provides more freedom in achieving design goals.

REFERENCES

1. O. Oralkan, A.S. Ergun, J.A. Johnson, M. Karaman, U. Demirci, K. Kaviani, T.H. Lee, and B.T. Khuri-Yakub, "Capacitive Micromachined Ultrasonic Transducers: Next-Generation Arrays for Acoustic Imaging?," *IEEE Trans. Ultrason., Ferroelect., Freq. Contr.*, vol. 49, pp. 1596-1610, November 2002.
2. I. Ladabaum, Xuecheng Jin, H. T. Soh, A. Atalar, and B. T. Khuri-Yakub, "Surface micromachined capacitive ultrasonic transducers," *IEEE Trans. Ultrason., Ferroelect., Freq. Contr.*, vol. 45, pp. 678-690, May 1998.
3. G.G. Yaralioglu, Mohammed H. Badi, A. Sanli Ergun, and Butrus T. Khuri-Yakub, "Improved equivalent circuit and finite element method modeling of capacitive micromachined ultrasonic transducers," Ultrasonics, 2003 IEEE Symposium on, Vol. 1, pp. 469-472, 5-8 Oct. 2003.

4. A. Lohfink, P.-C Eccardt, W. Benecke, and H. Meixner, “Derivation of a 1D CMUT model from FEM results for linear and nonlinear equivalent circuit simulation,” Ultrasonics, 2003 IEEE Symposium on, Vol. 1 , pp. 465-468, 5-8 Oct. 2003.
5. A. Bozkurt, I. Ladabaum, A. Atalar, and B.T. Khuri-Yakub, “Theory and analysis of electrode size optimization for capacitive microfabricated ultrasonic transducers”, IEEE Trans. Ultrason., Ferroelect., Freq. Contr., vol. 46, pp. 1364-1374, November 1999.
6. B. Bayram, G.G. Yaralioglu, A.S. Ergun, and B.T. Khuri-Yakub, “Influence of the electrode size and location on the performance of a CMUT,” Ultrasonics, 2001 IEEE Symposium on, Vol. 2 , pp. 949-952, 7-10 Oct. 2001.
7. G.G. Yaralioglu, A.S. Ergun, B. Bayram, E. Haeggstrom, and B.T. Khuri-Yakub, “Calculation and measurement of electromechanical coupling coefficient of capacitive micromachined ultrasonic transducers,” IEEE Trans. Ultrason., Ferroelect., Freq. Contr., vol. 50, pp. 449-456, April 2003.
8. B. Bayram, E. Haeggstrom, G.G. Yaralioglu, and B.T. Khuri-Yakub, “A new regime for operating capacitive micromachined ultrasonic transducers,” IEEE Trans. Ultrason., Ferroelect., Freq. Contr., vol. 50, pp. 1184-1190, September 2003.
9. Y. Roh, and B.T. Khuri-Yakub, “Finite Element Analysis of Underwater Capacitor Micromachined Ultrasonic Transducers,” IEEE Trans. Ultrason., Ferroelect., Freq. Contr., vol. 49, pp. 293-298, March 2002.
10. G. Wojcik, J. Mould, P. Reynolds, A. Fitzgerald, P. Wagner, and I. Ladabaum, “Time-domain models of MUT array cross-talk in silicon substrates,” Ultrasonics, 2000 IEEE Symposium on, Vol 1, pp. 909-914, Oct. 2000.
11. S. Ballandras, A. Caronti, W. Steichen, M. Wilm, V. Laude, T. Pastureaud, R. Lardat, and W. Daniau, “Simulation of cMUT radiating in water using a mixed finite element/boundary element approach,” Ultrasonics, 2002 IEEE Symposium on, Vol 2, pp. 1048-1051, Oct. 2002.
12. M. Kaltenbacher, H. Landes, K. Niederer, and R. Lerch, “3D simulation of Controlled Micromachined Capacitive Ultrasound Transducers,” Ultrasonics, 1999 IEEE Symposium on, Vol 2, pp. 1155-1158, Oct. 1999.
13. Y. Huang, A.S. Ergun, E. Haeggstrom, B.T. Khuri-Yakub, “Fabricating capacitive micromachined ultrasonic transducers with wafer-bonding technology,” J. Microelectromechanical Systems, Vol. 12, Iss. 2, pp. 128-137, April 2003.
14. V.L. Spiering, S. Bouwstra, R.M.E.J. Spiering, “On-chip decoupling zone for package-stress reduction,” Sensors and Actuators, Vol. 39, pp. 149-156, 1993.
15. Yongli Huang, Montreal.